Acta Crystallographica Section B
Structural Science
ISSN 0108-7681

Kinetic behaviour investigations and crystal structure of nitric acid dihydrate

N. Lebrun,[a]* F. Mahe,[b] J. Lamiot,[a] M. Foulon,[a] J. C. Petit[b] and D. Prevost[a]

[a]Laboratoire de Dynamique et Structure des Matériaux Moléculaires (UPRESA 8024), Université des Sciences et Technologies de Lille, UFR de Physique, Bâtiment P5, 59655 Villeneuve d'Ascq CEDEX, France, and [b]Laboratoire de Combustion et Systèmes Réactifs, CNRS, 1c avenue de la Recherche Scientifique, 45071 Orléans CEDEX 2, France

Correspondence e-mail: nathalie.lebrun@univ-lille1.fr

Received 19 June 2000
Accepted 26 October 2000

X-ray powder diffraction experiments are performed to prove the possible crystallization of nitric acid dihydrate ($HNO_3{\cdot}2H_2O$, further denoted NAD) and to determine the best thermal conditions for growing a single crystal. It is shown that the kinetic behaviour of NAD strongly depends on the preliminary thermal treatment. One good single crystal obtained by an *in situ* adapted Bridgman method procedure enabled determination of the crystal structure. The intensities of diffracted lines with h odd are all very weak. The H atom of nitric acid is delocalized to one water molecule leading to an association of equimolar nitrate (NO_3^-) and an $H_5O_2^+$ ionic group. The asymmetric unit contains two such molecules. These two molecules are related by a pseudo $a/2$ translation (with a 0.3 Å mean atomic distance difference), except for one H atom of the water molecules (0.86 Å) because of their different orientations in the two molecules. The two molecules, linked by very strong hydrogen bonds, are arranged in layers. Two layers which are linked by weaker hydrogen bonds are approximately oriented along the c axis. The structure may be described by translations of this set of two layers along the c axis without hydrogen bonds leading to a two-dimensional hydrogen-bond network. The structures of the monohydrate (NAM) and trihydrate (NAT) are redetermined for comparisons. These structures may be described by one- and three-dimensional hydrogen-bond networks, respectively.

1. Introduction

It is now well established that polar stratospheric clouds (PSCs) are the support for heterogeneous reactions responsible for the ozone depletion at the poles (Solomon, 1988). One of the most important classes of PSCs (type I PSCs) is formed during winter ($T \leq 200$ K) and consists mainly of nitric acid and water. The study of the composition, physical states and mechanisms of formation of these clouds is of paramount importance for a better understanding of the chemistry of ozone depletion. This requires a more accurate knowledge of the behaviour of some hydrates, particularly as regards equilibrium and non-equilibrium phase diagrams and also the kinetics and crystalline structures of their different solid phases.

Two hydrates, NAM (nitric acid monohydrate: $HNO_3{\cdot}H_2O$) and NAT (nitric acid trihydrate: $HNO_3{\cdot}3H_2O$) were first identified by Pickering (1893) using thermal analysis. The existence of these defined compounds was confirmed by Kuster & Kremann (1904) and later by Biltz *et al.* (1935).

The crystal structures of NAM and NAT were first determined by Luzzati (1951*b*, 1953). They were re-investigated for

greater precision, particularly concerning the descriptions of the hydrogen-bond network.

NAM (Delaplane *et al.*, 1975) crystallizes in an orthorhombic structure with $P2_1cn$ space group. The lattice parameters were measured at 85 K: a = 5.4647 (1), b = 8.6439 (1), c = 6.2308 (1) Å; and at 225 K: a = 5.4759 (2), b = 8.7242 (2), c = 6.3275 (2) Å.

NAT (Taesler *et al.*, 1975) is orthorhombic with space group $P2_12_12_1$. The cell parameters were measured at 85 K: a = 9.4845 (4), b = 14.6836 (9), c = 3.4355 (2) Å.

Toon et al. (1986), Hansen & Mauersberger (1988), Tolbert & Middlebrook (1990) and Arnold (1992) state that crystalline NAT should be the fundamental constituent of type I PSCs.

Solid NAM was also considered by Fahey *et al.* (1989) as another possible constituent. More recently, this view has been questioned (Toon & Tolbert, 1995) and the formation of nitric acid dihydrate (NAD) has been suggested (Ritzhaupt & Devlin, 1991; Worsnop *et al.*, 1993).

Recently, Ji & Petit (1992, 1993) and Mahé (1999) have reinvestigated, by DSC, the phase diagram in the concentration and temperature ranges of polar stratospheric cloud formation. Using the Tamann diagram they proved that NAD ($HNO_3{\cdot}2H_2O$) may crystallize after particular thermal treatments and that its behaviour strongly depends on the preliminary thermal treatment. The equilibrium phase diagram, measured from preliminary samples previously quenched in liquid nitrogen, showed that NAD undergoes a non-congruent reaction: NAD $\leftrightarrow$ NAT + liquid at 230 K (Fig. 1). On the contrary, the non-equilibrium phase diagram measured from samples previously slowly cooled (5 K min^{-1}) showed the congruent melting of NAD at 235 K (T_m in Fig. 1). Higher cooling rates ($\geq$ 10 K min^{-1}) led to the crystallization of NAM and NAT.

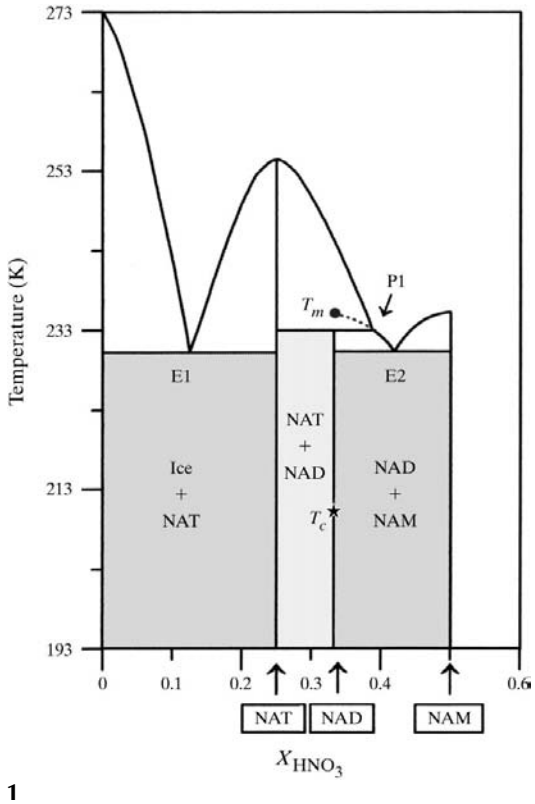

Figure 1
Phase diagram of HNO_3/H_2O mixtures [$0 < X(HNO_3) < 0.6$].

Preliminary X-ray powder diffraction studies (Ji *et al.*, 1996) using a Guinier–Simon camera confirmed the existence of solid NAD at the composition $X(HNO_3)$ = 0.35, but the diffraction diagrams were not accurate enough to determine its crystallographic characteristics.

Our work is devoted to the study of the kinetic behaviour of NAD using the X-ray powder diffraction technique from which the best thermal conditions to grow an *in situ* single crystal on the automatic four-circle diffractometer will be deduced. The crystal is of sufficiently good quality for its structure determination. The structure will be described and compared to those of nitric acid HNO_3, NAM and NAT.

2. Experimental

Commercial dilute nitric acid (68 wt %) was purchased from PROLABO RECTAPUR. The $HNO_3{\cdot}2H_2O$ mixture was prepared by mass dilution using bidistilled water. The concentration was controlled by acidimetry.

Thermal treatments were performed using a cryostream cooler (from Oxford Instruments) which operates from 80 to 373 K with a 0.1 K temperature stability.

2.1. Powder diffraction

The kinetic behaviour of NAD was investigated by X-ray powder diffraction. Approximately 3 mm^3 of liquid $HNO_3{\cdot}2H_2O$ was introduced by capillarity in a Lindemann cylindrical glass tube (φ = 0.7 mm). The glass capillary was further sealed by flame.

The sample rotated continuously around a vertical axis and was illuminated by a collimated (φ = 0.8 mm) monochromatic beam, Cu $K\alpha_1$ (λ = 1.54056 Å). The diffracted X-ray intensities were measured by means of a curved multidetector INEL CPS 120 and registered by a multichannel counter. Data were stored in a personal computer and fitted using Gaussian functions with asymmetric contributions. Experimental X-ray diagrams were corrected from scattering by air and container. Accurate calibration of the diffraction instrument was performed thanks to pure standards. The cubic material silicon (a = 5.43082 Å; Straumanis & Aka, 1952) and NAF ($Na_2Ca_3Al_2F_{14}$; a = 10.2498 Å; Courbion & Ferey, 1988) cover a large angular domain ($12 < 2\theta < 110^\circ$). The cubic material silver behenate (a = 58.376 Å; Blanton *et al.*, 1995) was also used for calibration at low diffraction angles ($0 < 2\theta < 20^\circ$).

2.2. Crystallographic studies on a single crystal

Crystal data and important parameters for the data collection and structure refinement of NAD are given in Table 1.[1] The cell parameters were refined from 25 reflections carefully

[1] Supplementary data for this paper are available from the IUCr electronic archives (Reference: GS0002). Services for accessing these data are described at the back of the journal.

Table 1
Experimental details.

Crystal data	
Chemical formula	$HNO_3{\cdot}2H_2O$
Chemical formula weight	99.04
Cell setting, space group	Monoclinic, $P2_1/n$
a, b, c (Å)	17.509 (3), 7.619 (4), 6.253 (3)
β (°)	107.5 (3)
V (Å^3)	796 (2)
Z	8
D_x (Mg m^{-3})	1.654
Radiation type	Mo $K\alpha$
No. of reflections for cell parameters	25
θ range (°)	5.5–25
μ (mm^{-1})	0.186
Temperature (K)	200
Crystal form, colour	Cylindrical, colourless
Crystal radius (mm)	0.5
Data collection	
Diffractometer	Philips PW1100
Data collection method	ω–2θ scans
Scan width (°)	1.5
Scan speed (° s^{-1})	0.04
No. of measured, independent and observed parameters	3665, 1567, 1315
Criterion for observed reflections	$I > \sigma(I)$
R_{int}	0.0417
θ_{max} (°)	26.03
Range of h, k, l	$-21 \rightarrow h \rightarrow 20$ $-9 \rightarrow k \rightarrow 9$ $-3 \rightarrow l \rightarrow 7$
No. and frequency of standard reflections	3 every 60 min
Intensity decay (%)	1
Refinement	
Refinement on	F^2
$R[F^2>2\sigma(F^2)]$, $wR(F^2)$, S	0.0324, 0.092, 1.434
No. of reflections and parameters used in refinement	1567, 150
H-atom treatment	Only H-atom U's refined
Weighting scheme	$w = 1/[\sigma^2(F_o^2) + (0.0375P)^2]$, $P = (F_o^2 + 2F_c^2)/3$
$(\Delta/\sigma)_{max}$	0.003
$\Delta\rho_{max}$, $\Delta\rho_{min}$ (e Å^{-3})	0.3, −0.2
Extinction method	*SHELXL*93 (Sheldrick, 1993)
Extinction coefficient	0.040 (4)

Computer programs used: Philips PW1100 Software, *SHELXS*86 (Sheldrick, 1985), *SHELXL*93 (Sheldrick, 1993), *ORTEP*III (Burnett & Johnson, 1996).

centred on the diffractometer. The intensities of three standard reflections were measured every hour. No correction was applied because of random and weak intensity fluctuations. Intensities were measured by the ω–2θ scanning mode. Left and right backgrounds were measured over half the scan time. Standard deviations on intensities were deduced from counting statistics. All the data were corrected for Lorentz–polarization factors. A secondary extinction correction was performed. Scattering factors of neutral atoms were approximated by exponential series from *International Tables for X-ray Crystallography* (1974, Vol. IV) and for H atoms from Stewart *et al.* (1965). Attempts to take into account the ionization of nitrate and oxonium groups led to no significant improvement in the results.

All calculations were performed on a Unix machine. The programs used are reported in Table 1. The structure was solved by direct methods using *SHELXS*86 (Sheldrick, 1985) and refined by full-matrix least-squares on F^2 using *SHELXL*93 (Sheldrick, 1993). After anisotropic refinement of the non-H atoms, all H atoms were located on a difference Fourier map (ρ = 0.5 e Å^{-3}). They were refined freely with isotropic displacement parameters in the final refinement cycles. The final refinement leads to a good reliability R factor equal to 0.0323. The illustration of the molecular arrangement was obtained using *ORTEP*III (Burnett & Johnson, 1996).

3. Results and discussion

3.1. Powder diffraction studies: kinetic studies of the crystallization of NAD under different thermal treatments

The crystallization of NAD was observed by Ji & Petit (1992, 1993) at 210 K (T_c in Fig. 1). Our experiments were performed on a mixture [$X(HNO_3)$ = 0.342] close to the NAD composition. We discuss here two particular thermal treatments among numerous others.

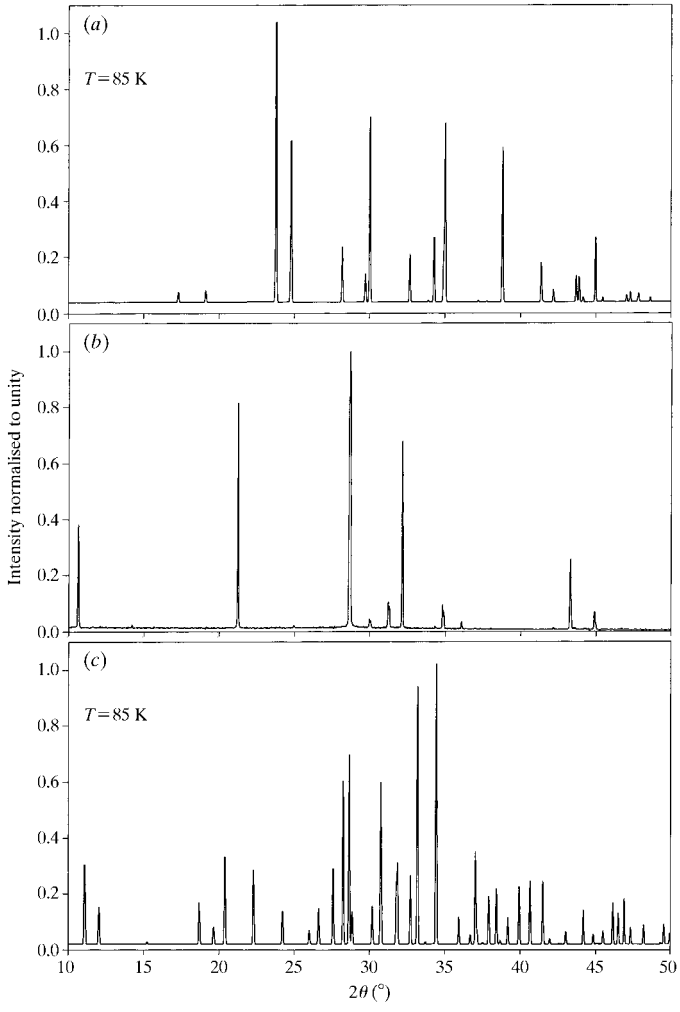

Figure 2
X-ray diffraction patterns: (*a*) calculated for nitric acid monohydrate (NAM) from Delaplane *et al.* (1975); (*b*) experimental for nitric acid dihydrate (NAD) measured after 30 min at 200 K (experiment 1); (*c*) calculated for nitric acid trihydrate (NAT) from Taesler *et al.* (1975).

3.1.1. First experiment. The liquid was quenched from 293 to 200 K by quick translation of the capillary in a cold gas flow. A sudden crystallization was observed. During all the following thermal treatments, X-ray diffraction patterns were registered every 30 min.

(i) The compound was first maintained under isothermal conditions for 200 min.

The X-ray diagram recorded during the first half an hour at 200 K (Fig. 2*b* and Fig. 3, part *B*) was compared to the simulated one for NAT (Fig. 2*c*) and NAM (Fig. 2*a*) deduced from the known structures. For greater clarity, all the diffracted intensities were normalized to unity in Fig. 2. This compound clearly crystallizes first into another solid, then NAT and (or) NAM.

Few diffracted lines were observed and the solid crystal was very transparent. This proves that the liquid crystallized as large monocrystalline domains with a preferential orientation. All attempts to determine the cell parameters, by trial-and-error procedures, failed.

This solid is identified as the stable phase of NAD at low temperature after structure determination.

After annealing for 1 h, some new weak diffracted lines appear (Fig. 3, part *B*). They show the crystallization of a small amount of NAT, which does not increase throughout the isothermal period. This implies that some nuclei were formed during this preliminary thermal treatment. For stoichiometric reasons, the crystallization of a small amount of NAM may be expected but is not observed throughout the isothermal period. One interpretation is that a small part of the starting compound remains as a metastable liquid, leading to a scattering ring which is too low and therefore unobservable.

Table 2
Selected intramolecular geometric parameters (Å, °).

Molecule *A*		Molecule *B*	
N*A*—O1*A*	1.286 (2)	N*B*—O1*B*	1.279 (2)
N*A*—O2*A*	1.222 (2)	N*B*—O2*B*	1.223 (2)
N*A*—O3*A*	1.235 (2)	N*B*—O3*B*	1.253 (2)
O4*A*—H1*A*	0.99 (3)	O4*B*—H1*B*	0.92 (3)
O4*A*—H2*A*	0.93 (2)	O4*B*—H2*B*	0.91 (3)
O4*A*—H3*A*	0.81 (3)	O4*B*—H3*B*	0.85 (2)
O5*A*—H4*A*	0.88 (3)	O5*B*—H4*B*	0.99 (3)
O5*A*—H5*A*	0.83 (3)	O5*B*—H5*B*	0.78 (2)
O1*A*—N*A*—O2*A*	119.2 (1)	O1*B*—N*B*—O2*B*	119.7 (1)
O1*A*—N*A*—O3*A*	117.4 (1)	O1*B*—N*B*—O3*B*	118.0 (1)
O2*A*—N*A*—O3*A*	123.5 (1)	O2*B*—N*B*—O3*B*	122.3 (1)
H1*A*—O4*A*—H2*A*	111 (2)	H1*B*—O4*B*—H2*B*	111 (2)
H1*A*—O4*A*—H3*A*	117 (2)	H1*B*—O4*B*—H3*B*	114 (2)
H2*A*—O4*A*—H3*A*	108 (2)	H2*B*—O4*B*—H3*B*	110 (2)
H4*A*—O5*A*—H5*A*	108 (3)	H4*B*—O5*B*—H5*B*	105 (2)

(ii) The compound is then reheated up to 243 K at a constant 0.07 K min^{-1} rate.

Fig. 3 shows the diffracted diagrams every 1 K from 223 K (part *C*) to 229 K (part *I*). No important significant modification was observed up to 223 K.

The diffracted lines of NAD began to decrease at 223 K. This was followed by crystallization of NAM at ∼224 K (part *D*) certainly due to a so-called 'cold crystallization' process. NAD and NAM disappear completely at ∼226 K (part *F*) and 228 K (part *H*), respectively. A significant increase in the diffracted intensities of NAT (part *E*) is simultaneously observed which begins at 225 K. The melting of NAT is observed at 252 K. These results agree well with the equilibrium phase diagram (Ji & Petit, 1992, 1993; Mahé, 1999).

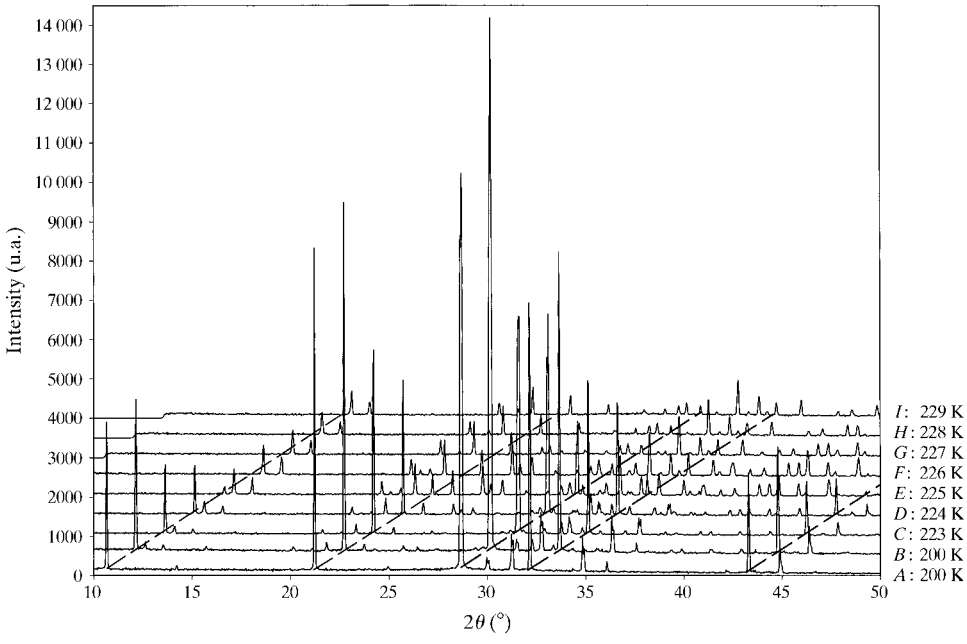

Figure 3
X-ray patterns recorded after quenching from 293 K down to 200 K. The two lower diagrams are taken at 200 K after (part *A*) half an hour and (part *B*) 1 h, respectively. X-ray patterns are shifted in 2θ and in intensity. Dotted lines show the intensity decrease in the most important diffracted lines of NAD.

3.1.2. Second experiment. This experiment is performed in order to avoid the 'parisitic' crystallization of NAT and NAM owing to their nucleations during an isothermal period at 200 K. The same sample was quenched down to 200 K as in the first experiment, but was immediately and rapidly reheated at a 6 K min^{-1} rate up to 213 K.

The X-ray diffraction pattern measured after 30 min at 213 K is depicted in Fig. 4 and compared with that obtained during the previous experiment at 200 K, and a diagram calculated from the single-crystal structure analysis. The diffracted intensities were normalized to unity. The solid is not as transparent as for the first experiment and more diffracted lines were observed, but the determination of the crystallographic parameters using

trial-and-error computing programs also fails.

The compound was then heated from 213 K up to 243 K at 0.07 K min^{-1}. In contrast to the first experiment, no transformation occurs during heating. Only the congruent melting of NAD is observed at 233 K, in agreement with the phase diagram (Fig. 1) determined by Ji & Petit (1992, 1993) using samples previously cooled slowly (5 K min^{-1}).

3.1.3. Best thermal conditions for single-crystal growth. These experiments clearly confirm the possible crystallization of NAD and that the thermal behaviour of NAD strongly depends on the preliminary thermal treatment. They also indicate the best thermal conditions in which to grow a single crystal.

The same NAD crystalline phase is observed in both experiments, but some discrepancies are observed in the magnitude of certain diffracted intensities. Furthermore, the reflections (*hkl*) with *k* non-equal zero are systematically absent (first experiment) or weak (second experiment, see Fig. 4). This is clearly due to a preferential axial crystallization with the *b* axis along the axis of the rotating vertical capillary parallel to the cold gas flow. This may be favoured by the low-temperature gradient.

Table 3
Hydrogen-bond geometries (Å, °).

Bond description	$d_{O\cdots O}$ (Å)	$d_{O\cdots H}$ or $d_{H\cdots O}$ (Å)	$\theta_{O-H\cdots O}$ (°)
Hydrogen bonds linking the two ions (nitrate and oxonium) and the water molecule in the two molecules *A* and *B*			
O4*A*—H1*A*···O1*A*^{i}	2.550 (2)	1.55 (3)	172 (3)
O4*B*—H1*B*···O1*B*^{i}	2.606 (2)	1.69 (3)	174 (3)
O4*A*—H2*A*···O5*A*^{i}	2.559 (2)	1.64 (2)	174 (2)
O4*B*—H2*B*···O5*B*^{i}	2.460 (2)	1.55 (3)	176 (2)
Hydrogen bonds linking the two molecules *A* and *B* in an independent group			
O5*A*—H4*A*···O3*B*^{i}	2.828 (2)	1.96 (3)	169 (3)
O5*B*—H4*B*···O3*A*^{i}	2.768 (2)	1.79 (3)	168 (3)
Hydrogen bonds linking the independent groups in one layer			
No. 1: O4*B*—H3*B*···O1*A*^{ii}	2.628 (2)	1.79 (2)	167 (2)
No. 2: O4*A*—H3*A*···O1*B*^{iii}	2.604 (2)	1.80 (2)	169 (2)
No. 3: O5*B*—H5*B*···O5*A*^{iv}	2.822 (2)	2.06 (3)	167 (3)
Hydrogen bonds linking the two layers of molecules			
No. 4: O5*A*—H5*A*···O3*B*^{v}	2.940 (2)	2.14 (3)	162 (2)

Symmetry codes: (i) x, y, z; (ii) $\frac{1}{2}+x, \frac{1}{2}-y, \frac{1}{2}+z$; (iii) $-\frac{1}{2}+x, -\frac{1}{2}-y, -\frac{1}{2}+z$; (iv) $x, 1+y, z$; (v) $\frac{3}{2}-x, -\frac{1}{2}+y, -z$.

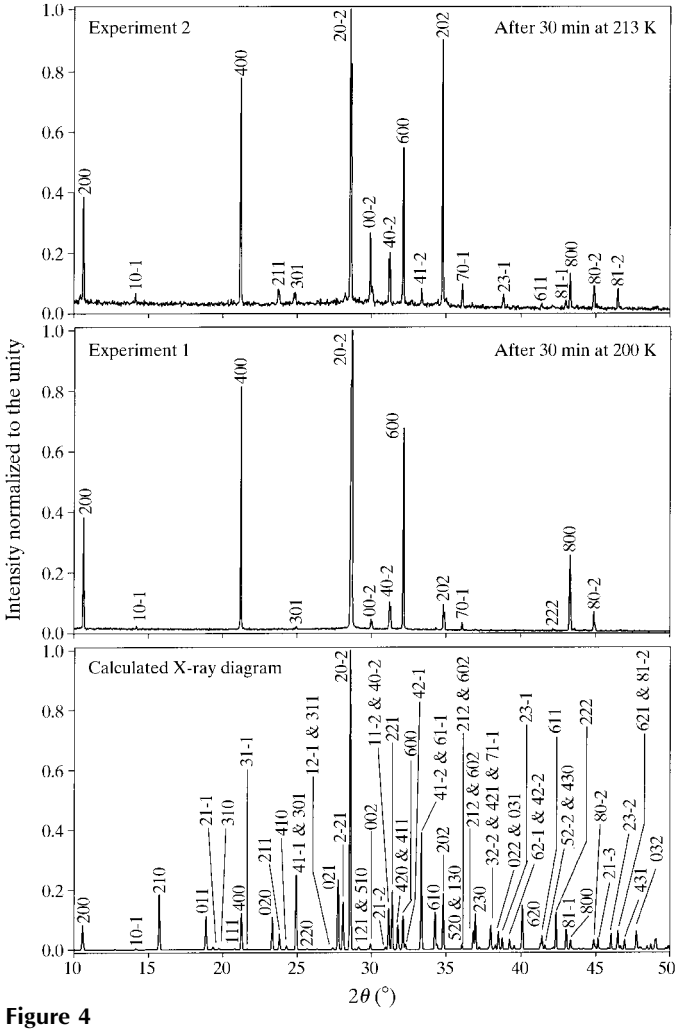

Figure 4
X-ray diffraction patterns for NAD after a 30 min annealing at 200 and 213 K compared with the calculated one at 200 K.

The first method is to quench the liquid down to 200 K and to grow the single crystal at this temperature. The growing of large monocrystalline domains with a preferential orientation is certainly a favourable factor. At this temperature the amount of crystalline NAT is very low and the diffracted intensities of NAD may be registered at this temperature.

The second method is to quench the liquid at 200 K and to grow the crystal at 213 K after rapid reheating. This seems to avoid any other crystallization, but the mono-crystalline domains are certainly not as large as in the first experiment.

3.2. Single-crystal diffraction studies

3.2.1. Single-crystal growth and behaviour on re-heating. For single-crystal analysis, liquid nitric acid dihydrate is introduced by capillarity into a Lindemann tube (φ = 0.5 mm; height of liquid: 10 mm). The capillary is sharpened in its upper part in order to favour the growth of a single crystal from a little small germ. The single crystal is grown *in situ* on the four-circle Philips PW1100 diffractometer using an adapted Bridgman method.

The liquid is quenched from 293 K down to 200 K as in the first powder diffraction experiment. It crystallizes rapidly into a solid which is then partially melted by horizontal displacement of the capillary in a temperature gradient thanks to the outer de-icing warm stream (285 K) and the inner cold one (at 200 K) of the low-temperature device. A very small crystalline germ is kept in the sharpened extremity of the capillary. The liquid part is moved very slowly towards the low-temperature (200 K) stream. The single-crystal growth from the little germ is checked by visual observation of the solid–liquid frontier displacement thanks to a binocular telescope. The quality of the single crystal is checked by controlling the profile of some diffracted lines chosen in different 'regions' of the reciprocal

Table 4
Geometry of the NO_3 group or ion in some selected compounds.

	N—O1 (Å)	N—O2 (Å)	N—O3 (Å)	O1—N—O3 (°)	O1—N—O2 (°)	O2—N—O3 (°)
NO_3 in gaseous	1.22	1.22	1.41	115.0	130.0	115.0
nitric acid (*a*), (*b*)	1.21	1.20	1.41	115.7	130.2	114.1
NO_3 in solid	1.28	1.19	1.21	117	130	113
nitric acid (*c*)	1.21	1.22	1.33	113	138	109
	1.20	1.25	1.31	119	140	101
	1.26	1.25	1.25	116	134	110
NO_3^- in NAM (*d*)	1.254	1.258	1.257	119.4	120.5	120.1
($HNO_3{\cdot}H_2O$) (*e*)	1.252 (2)	1.251 (2)	1.249 (1)	119.9 (1)	120.0 (1)	120.0 (1)
NO_3^- in NAD ($HNO_3{\cdot}2H_2O$)						
Molecule *A* (*e*)	1.286 (2)	1.222 (2)	1.235 (2)	117.4 (1)	119.2 (1)	123.5 (1)
Molecule *B* (*e*)	1.279 (2)	1.223 (2)	1.253 (2)	118.0 (1)	119.7 (1)	122.3 (1)
NO_3^- in NAT (*f*)	1.247	1.265	1.256	121.2	120.3	118.5
($HNO_3{\cdot}3H_2O$) (*e*)	1.244 (1)	1.252 (1)	1.251 (1)	120.7 (1)	120.7 (1)	118.5 (1)

(*a*) Maxwell & Mosley (1940); (*b*) Cox *et al.* (1994); (*c*) Luzzati (1951*a*); (*d*) Delaplane *et al.* (1975); (*e*) our work; (*f*) Taesler *et al.* (1975).

Table 5
Geometry of the oxonium H_3O^+ ion in solid NAM, NAD and NAM after refinement of H coordinates (from our work).

	O—H1 (Å)	O—H2 (Å)	O—H3 (Å)	H1—O—H2 (°)	H1—O—H3 (°)	H2—O—H3 (°)
NAM	0.93 (3)	0.87 (3)	0.97 (4)	103 (3)	107 (3)	115 (3)
NAD						
Molecule *A*	0.99 (3)	0.93 (2)	0.81 (3)	111 (2)	117 (2)	108 (2)
Molecule *B*	0.92 (3)	0.91 (3)	0.85 (2)	111 (2)	114 (2)	110 (2)
NAT	0.82 (3)	0.86 (3)	0.88 (3)	105 (3)	115 (2)	103 (3)

lattice and by measuring the diffracted intensities of some equivalent lines. After some failing unsuccessful attempts, the crystal is of sufficient quality to permit a data collection.

The crystal is finally slowly reheated. No other crystallization or transformation is observed. Contrary to the first powder diffraction experiment, the congruent melting of NAD is observed at approximately 233 K. This is due to the *in situ* growth from a liquid which avoids the nucleation of NAT and NAM during the rapid growth of NAD from a little small germ by translation in a large temperature gradient.

3.2.2. Molecular structure and crystal packing. Molecular structure: The asymmetric unit contains two independent ($H_5O_2^+{\cdot}NO_3^-$) molecules named *A* and *B*.

The delocalization of the nitric acid hydrogen to one water molecule leads to the formation of a nitrate ion NO_3^-, an oxonium ion H_3O^+ and a water molecule linked together by strong hydrogen bonds.

The characteristics of covalent and hydrogen bonds linking molecules *A* and *B* are given for the two independent molecules in Tables 2 and 3.

Applying the inversion symmetry to molecule *B* shows that the two independent molecules are related by a pseudo-translation *a*/2, explaining that the diffracted intensities for (*hkl*) planes are (very) weak for odd *h* values. The mean distance between corresponding atoms is low (0.3 Å), except for one H atom (H5*A* and H5*B*, 0.86 Å) of the water molecules because of the different orientations in the two molecules.

The nitrate NO_3^- ions are planar but deviate from the expected ternary symmetry. For the two molecules *A* and *B*, one N—O bond (N*A*—O1*A* and N*B*—O1*B*) is significantly longer than the two others because of a strong hydrogen bond linking one acceptor oxygen (O1*A* or O1*B*) atom of the nitrate ion to an H donor atom (H1*A* or H1*B*) of the H_3O^+ ion. The water molecule is also strongly linked, *via* its acceptor O atom (O5*A* or O5*B*), to the H_3O^+ group involving one other H (H2*A* or H2*B*) donor atom, leading to an asymmetrical $H_5O_2^+$ ion. These 'intramolecular' strong hydrogen bonds have practically the same geometrical characteristics with the following mean values: $d(O\cdots O)$ = 2.54 Å (0.05) and $d(O\cdots H)$ = 1.62 Å (0.06) and O—H$\cdots$O = 174.3° (1.4).

The *A* and *B* molecules are linked together by a weaker but nevertheless strong hydrogen bond involving one other O atom (O3*A* or O3*B*) of the nitrate ion as an acceptor to one other donor hydrogen (H4*A* or H4*B*) atom of the H_3O^+ group.

The association of the two molecules (*A* and *B*) described above will be further named the independent group in the following.

Crystal packing: The solid-state packing is mainly governed by hydrogen bonds between NO_3^- and $H_5O_2^+$ ions of the independent groups. They are arranged in groups of two infinite puckered layers named L_1 and L_2 with the mean plane parallel to the $(10\bar{1})$ crystallographic plane.

L_1 is formed by independent groups related by the diagonal symmetry plane. L_2 is related to L_1 by the inversion symmetry. One such layer is depicted in Fig. 5, which shows a projection in the (101) crystallographic plane.

The linkage of the independent groups in one layer is ensured by a complicated two-dimensional hydrogen-bond network. The geometrical characteristics of the hydrogen bonds are given in Table 3. One molecule, for example *A*, is

linked to three *B* molecules belonging to adjacent groups by three different types of hydrogen bonds. The strong bond (denoted 1, Table 3) links the acceptor NO_3^- to one donor H_3O^+. The strong bond (denoted 2) links the donor H_3O^+ to one acceptor NO_3^-. A weaker hydrogen bond (denoted 3) links the water molecule which is an acceptor for molecule *A* and a donor for molecule *B* *via* the H5*B* atom.

The L_1 and L_2 layers (Fig. 6) are weakly linked by one type of hydrogen bond (denoted 4) involving the 'out-of-layer' H5*A* atom of the water molecule as a donor to the nitrate ion of molecule *B*.

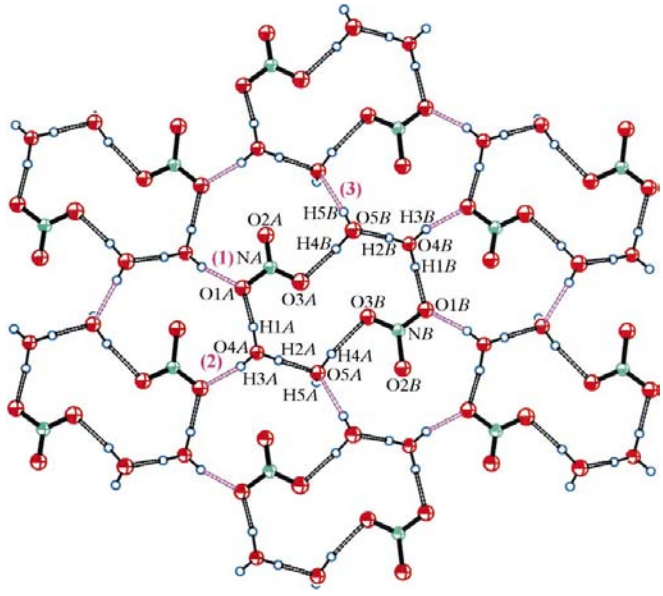

Figure 5
Projection along [001] of the two independent molecules (*A* and *B*), showing the numbering and their neighbourhood in one layer. Hydrogen bonds are indicated by double thin broken lines. Thermal ellipsoids for heavy atoms are drawn with a 50% probability level.

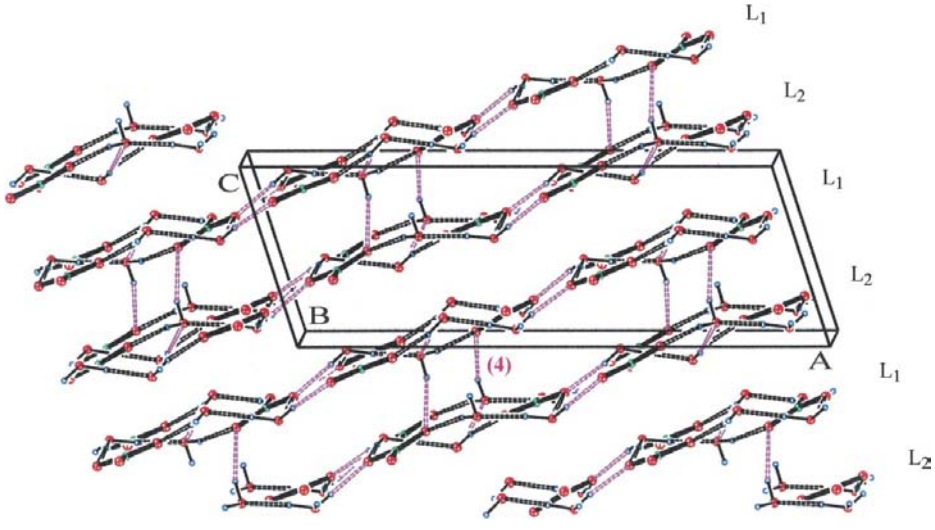

Figure 6
Projection along the [010] direction showing the two types of layers (L_1 and L_2) and the crystal packing of NAD.

The structure may be described by the translation of this group of two linked layers along the [001] direction (Fig. 6). These groups of two layers are not linked together.

From the point of view of interionic contacts, only two O atoms of the NO_3^- ions are engaged in three acceptor hydrogen bonds, explaining the N—O bond length differences. One O atom is strongly linked to two oxonium ions, while the second one is more weakly linked to a water molecule. The three donor H atoms of the oxonium H_3O^+ ions are linked by strong contacts with two NO_3^-ions and one water molecule.

The O atoms of the water molecules are strongly linked to oxonium ions, while the two H atoms are weakly linked to NO_3^- ions, in the layers for the *B* molecule and between two layers for the *A* molecule.

Comparison with other structures containing nitric acid: The crystal structures of the monohydrate NAM ($HNO_3{\cdot}H_2O$) and the trihydrate NAT ($HNO_3{\cdot}3H_2O$) were re-investigated in this study. Crystals were obtained by a similar *in situ* procedure. Our results confirm the previous studies and the crystal data obtained by Delaplane *et al.* (1975) for NAM and Taesler *et al.* (1975) for NAT. They crystallize in the orthorhombic system.

The cell parameters for NAM, at 200 K, are a = 6.317 (3), b = 8.723 (4), c = 5.477 (3) Å with space group $P2_1cn$ (R = 0.0302). The molecule is dissociated in NO_3^- and oxonium H_3O^+ ions. The H_3O^+ and NO_3^- ions exhibit a pseudo-threefold axis. The molecular arrangement, deduced from our structural data, is shown in Fig. 7. All O and H atoms are linked by hydrogen bonds. The oxonium ion (H_3O^+) is hydrogen bonded to three different nitrate ions to form one-dimensional infinite staggered layers, whose mean planes are parallel to the (100) crystallographic plane. The layers are symmetrically related by the helicoïdal twofold axis parallel to **a**. The layers are not related by hydrogen bonds.

The cell parameters for NAT (space group $P2_12_12_1$) at 220 K are a = 9.508 (3), b = 14.718 (4), c = 3.518 (3) Å (R = 0.0282). The molecular arrangement, deduced from our structural data, is shown in Fig. 8. The structure contains nitrate ions and oxonium H_3O^+ ions, each of which is bonded to two water molecules to form $H_7O_3^+$ ions. All O and H atoms are linked by hydrogen bonds. The $H_7O_3^+$ ions are linked to one another as helix helices which are hydrogen bonded to NO_3^- ions. The structure may be described by infinite staggered layers linked by hydrogen bonds leading to a three-dimensional network.

Finally, the two-dimensional network of molecular layers of NAD may be considered as intermediate between those of NAM (one-dimensional network) and NAT (three-dimensional network).

Concerning the NO_3 geometry, Table 4 contains data for HNO_3 in the gaseous state (Maxwell & Mosley, 1940; Cox *et al.*, 1994) as in the crystalline state (Luzzati, 1951*a*). The characteristics of the NO_3^- ions in crystals of NAM (Delaplane *et al.*, 1975; and our study), NAD (our study) and NAT (Taesler *et al.*, 1975; and our study) are also listed.

The geometry of NO_3 in pure nitric acid HNO_3 is naturally different from that of the NO_3^- ion in NAM, NAD and NAT. Pure nitric acid may be written as $(NO_2)OH$, explaining the asymmetrical geometry. In the gaseous and solid states, the N—O—H bond is naturally larger than the other two. The angle between these two N—O bonds is larger than the other two.

All the NO_3^- ions in the crystallized hydrated nitric acid are quasiplanar. The O—N—O angles are equal (approximately 120°) whatever the number of water molecules, but significant differences are observed in the lengths of the N—O bonds depending on the symmetry and number of strong contacts by hydrogen bonds. In NAM, each O atom is engaged in an identical hydrogen bond and the NO_3^- group exhibits an internal ternary symmetry. For NAD, the asymmetrical geometry of hydrogen bonds (§3.2.2) leads to important deviations from the ternary symmetry of NO_3^-. For NAT, the NO_3^- recovers its quasi-ternary symmetry due to symmetrical contacts.

For all solid phases, the oxonium H_3O^+ roughly agrees with a C_{3v} symmetry (Table 5).

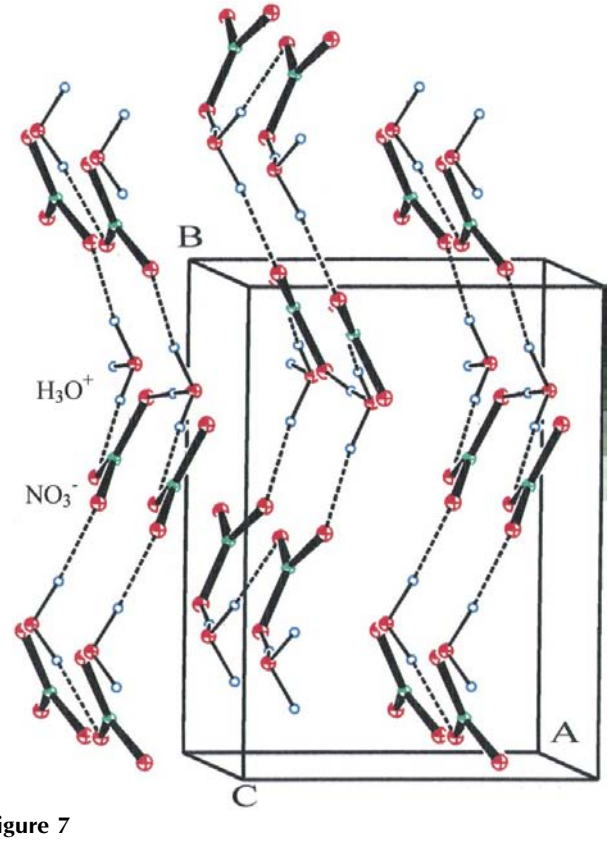

Figure 7
Projection approximately along the [001] direction showing the crystal packing of NAM.

G. Odou and F. Danède are gratefully acknowledged for their help and for their skilled technical assistance. This project was supported by a grant from the National Program of the Chemistry of the Atmosphere.

References

Arnold, F. (1992). *Ber. Bunsenges. Phys. Chem.* **3**, 339–350.
Biltz, W., Hülsmann, O. & Eickholtz, W. (1935). *Nachr. Gotting. Ges.* **2**, 95–102.
Blanton, T. N., Huang, T. C., Toraya, H., Hubbard, C. R., Robie, S. B., Louër, D., Göbel, H. E., Will, G., Gilles, R. & Raftery, T. (1995). *Powder Diffr.* **10-2**, 91–95.
Burnett, M. N. & Johnson, C. K. (1996). *ORTEP*III. Report ORNL-6895. Oak Ridge National Laboratory, Tennessee, USA.
Courbion, G. & Ferey, G. (1988). *J. Solid State Chem.* **76**, 426–431.
Cox, A. P., Ellis, M. C., Attfield, C. J. & Ferris, A. C. (1994). *J. Mol. Struct.* **320**, 91–106.
Delaplane, R. G., Taesler, I. & Olovsson, I. (1975). *Acta Cryst.* B**31**, 1486–1489.
Fahey, D. W., Kelly, K. K., Ferry, G. V., Poole, L. R., Wilson, J. C., Murphy, D. M., Loewenstein, M. & Chan, K. R. (1989). *J. Geophys. Res.* **94-11**, 299–315.

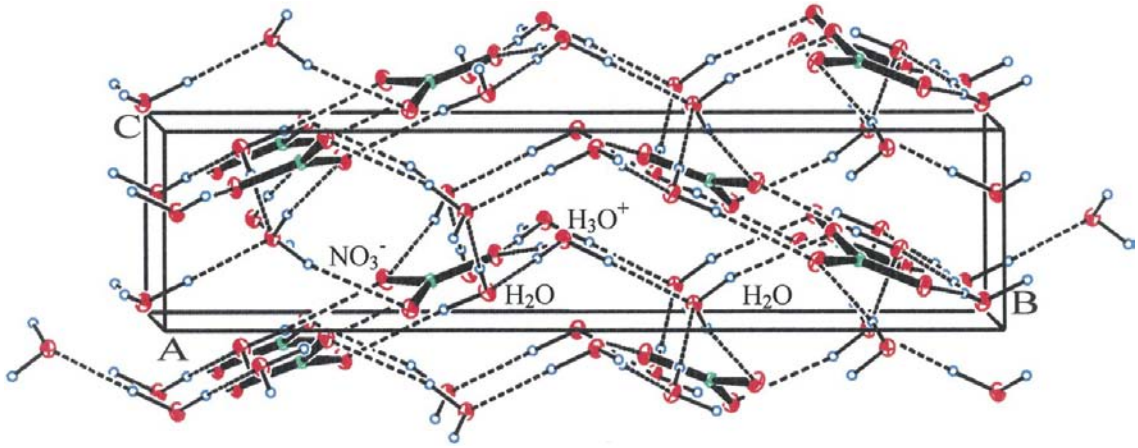

Figure 8
Crystal packing for the trihydrate NAT: projection approximately along the [100] direction illustrating the three-dimensional hydrogen-bond network.

Hansen, D. & Mauersberger, K. (1988). *J. Phys. Chem.* **92**, 6167–6170.
Ji, K. & Petit, J. C. (1992). *Air Pollut. Rep.* **42**, 162–165.
Ji, K. & Petit, J. C. (1993). *C. R. Acad. Sci. Paris*, **316-II**, 1743–1748.
Ji, K., Petit, J. C., Négrier, P. & Haget, Y. (1996). *Geophys. Res. Lett.* **23-9**, 981–984.
Kuster, H. & Kremann, R. (1904). *Z. Anorg. Chem.* **41**, 1–41.
Luzzati, V. (1951*a*). *Acta Cryst.* **4**, 120–131.
Luzzati, V. (1951*b*). *Acta Cryst.* **4**, 239–244.
Luzzati, V. (1953). *Acta Cryst.* **6**, 152–164.
Mahé, F. (1999). Thésis (12/1999). Orléans University, France.
Maxwell, L. R. & Mosley, V. M. (1940). *J. Chem. Phys.* **8**, 738–742.
Pickering, S. U. (1893). *J. Chem. Soc.* **63**, 436–443.
Ritzhaupt, G. & Devlin, J. P. (1991). *J. Phys. Chem.* **95**, 90–95.
Sheldrick, G. M. (1985). *SHELXS*86. University of Göttingen, Germany.
Sheldrick, G. M. (1993). *SHELXL*93. University of Göttingen, Germany.
Solomon, S. (1988). *Rev. Geophys.* **26**, 131–148.
Stewart, R. F., Davidson, E. R. & Simpson, W. T. (1965). *J. Chem. Phys.* **42-9**, 3175–3187.
Straumanis, M. E. & Aka, E. Z. (1952). *J. Appl. Phys.* **23**, 330–334.
Taesler, I., Delaplane, R. G. & Olovsson, I. (1975). *Acta Cryst.* B**31**, 1489–1492.
Tolbert, M. A. & Middlebrook, A. M. (1990). *J. Geophys. Res.* **95**, 22423–22431.
Toon, O. B., Hamill, P., Turco, R. P. & Pinto, J. (1986). *Geophys. Res. Lett.* **13**, 1284–1287.
Toon, O. B. & Tolbert, M. A. (1995). *Nature*, **375**, 218–221.
Worsnop, D. R., Fox, L. E., Zahniser, M. S. & Wolfsy, S. C. (1993). *Science*, **259**, 71–74.